

Evolution of spin excitations in a gapped antiferromagnet from the quantum to the high-temperature limit

M. Kenzelmann,¹ R. A. Cowley,¹ W. J. L. Buyers,^{2,3} R. Coldea,^{4,5} M. Enderle,^{6,7} and D. F. McMorrow⁸

¹*Oxford Physics, Clarendon Laboratory, Oxford OX1 3PU, United Kingdom*

²*Neutron Program for Materials Research, National Research Council of Canada, Chalk River, Ontario, Canada K0J 1J0*

³*Canadian Institute for Advanced Research*

⁴*Oak Ridge National Laboratory, Solid State Division, Oak Ridge, Tennessee 37831*

⁵*ISIS Facility, Rutherford Appleton Laboratory, Oxon OX11 0QX, United Kingdom*

⁶*Technische Physik, Gebäude 38, Universität des Saarlandes, D-66123 Saarbrücken, Germany*

⁷*Institut Laue-Langevin, Boîte Postal 156 38042 Grenoble, Cedex 9, France*

⁸*Condensed Matter Physics and Chemistry Department, Risø National Laboratory, DK-4000, Roskilde, Denmark*

(Received 10 December 2001; revised manuscript received 1 July 2002; published 8 November 2002)

We have mapped from the quantum to the classical limit the spin excitation spectrum of the antiferromagnetic spin-1 Heisenberg chain system CsNiCl_3 in its paramagnetic phase from $T=5$ to 200 K. Neutron scattering shows that the excitations are resonant and dispersive up to at least $T=70$ K $\approx 2.7J$, but broaden considerably with increasing temperature. The dispersion flattens out with increasing temperature as the resonance energy Δ at the antiferromagnetic wave vector increases and the maximum in the dispersion decreases. The correlation length ξ between $T=12$ and 50 K is in agreement with quantum Monte Carlo calculations for the spin-1 chain. ξ is also consistent with the single mode approximation, suggesting that the excitations are short-lived single particle excitations. Below $T=12$ K where three-dimensional spin correlations are important, ξ is shorter than predicted and the experiment is not consistent with the random phase approximation for coupled quantum chains. At $T=200$ K, the structure factor and second energy moment of the excitation spectrum are in excellent agreement with the high-temperature series expansion.

DOI: 10.1103/PhysRevB.66.174412

PACS number(s): 75.25.+z, 75.10.Jm, 75.40.Gb

I. INTRODUCTION

Low-dimensional antiferromagnets are ideal systems in which to investigate the effect of strong quantum fluctuations on the dynamics of interacting spin systems. Quantum fluctuations are similar to temperature fluctuations in three-dimensional (3D) magnets in that they disorder the spin system and prevent magnetic order. Similar to the paramagnetic phase of a 3D magnet, the quantum-disordered phase of a low-dimensional antiferromagnet has unbroken translational symmetry, but while the excitation spectrum of a 3D paramagnet consists of broad magnetic excitations, the elementary magnetic excitations of a low-dimensional antiferromagnet are either spin-1/2 or long-lived spin-1 particles.¹⁻³

One-dimensional (1D) antiferromagnets have been studied for at least the last 30 years. They were first perceived as simpler model systems than their 3D counterparts, but it is now clear that their low-temperature spin dynamics is far more complex. The quantum-disordered ground state of 1D antiferromagnets is usually a highly correlated spin singlet. Haldane, in his seminal 1983 paper, conjectured that the spin dynamics of 1D antiferromagnets crucially depends on the spin quantum number:² The half-integer spin Heisenberg antiferromagnet has a gapless excitation spectrum while integer-spin chains exhibit an energy gap. Haldane's conjecture of a spin-1 gap was then confirmed by numerical^{4,5} and experimental studies⁶⁻⁸ and is now generally accepted.

The low-temperature quantum-disordered ground state of the antiferromagnetic spin-1/2 chain is "almost ordered" and its correlations fall off with distance as a power law. The

elementary excitations form a broad continuum of spinons carrying spin-1/2 which correspond to moving domain walls between regions of coherent quantum states. In contrast, the correlations in antiferromagnetic spin-1 chains fall off exponentially with a correlation length of about six sites at zero temperature. The elementary excitations are massive triply degenerate spin-1 particles that give sharp Haldane excitations, which can be pictured as domain walls breaking the hidden spin string order that is inherent in spin-1 chains.⁹ The triplet excitations follow the relativistic dispersion of the nonlinear sigma model (NL σ M).¹⁰

The temperature dependence of the excitation spectrum of antiferromagnetic chains has been measured mostly for $T \leq J$, where J is the exchange interaction between the spins along the chain direction. For KCuF_3 , an antiferromagnetic spin-1/2 chain system with $J=17$ meV, inelastic neutron scattering up to $T=200$ K $\approx J$ showed that the low-energy excitations are broadened at high temperatures but can still be described by a low-temperature field theory.¹¹

For spin-1 chains, the temperature dependence of $S(\mathbf{Q}, \omega)$ has been investigated for CsNiCl_3 ,^{6,12,13} RbNiCl_3 ,¹² NENP ,⁸ NINAZ ,¹⁴ AgVP_2S_6 ,¹⁵ and Y_2BaNiO_5 ,¹⁶ and for temperatures T up to at most $T \sim J$. The temperature dependence of the excitation for $T < 0.3J$ was studied for AgVP_2S_6 and Y_2BaNiO_5 ($J=60$ meV and $J=24.1$ meV, respectively). These measurements give the behavior of the low-temperature quantum-disordered phase. A further inelastic neutron scattering study of AgVP_2S_6 showed that the staggered susceptibility decreases with increasing temperature up to $T=200$ K $\approx 0.3J$.¹⁷ A single crystal experiment on

Y_2BaNiO_5 showed that the energy gap observed by neutron scattering is renormalized upward with increasing temperature up to $T=80\text{ K}\approx 0.3J$.¹⁸

NINAZ, NENP, and CsNiCl_3 have smaller exchange interactions than AgVP_2S_6 and Y_2BaNiO_5 ($J=10.73\text{ meV}$, $J=4\text{ meV}$, and $J=2.28\text{ meV}$, respectively) and they were studied over a wider temperature range. The upward renormalization of the energy gap of the Haldane excitations and their damping was measured in NINAZ up to $T=50\text{ K}\approx 0.4J$ and in NENP up to $T=20\text{ K}\approx 0.43J$.¹⁹ The temperature dependence of the spin correlation length in NENP has been determined up to $T=100\text{ K}\approx 2J$.²⁰ The temperature dependence of the gap in CsNiCl_3 at the 3D ordering wave-vector was previously studied up to $T=20\text{ K}\approx 0.75J$,^{7,13} and at the 1D wave vector up to $T=12\text{ K}\approx 0.5J$.^{12,21}

Surprisingly a detailed study of the excitation spectrum of antiferromagnetic spin chains for $T>J$ and in the high-temperature limit has not been made. We showed recently that the Haldane gap in CsNiCl_3 persists as a resonant feature up to at least $T=70\text{ K}$ or $2.7J$.²² Here we present more extensive measurements at low and high temperatures including a comprehensive study of the spin dynamics of the 1D magnet for temperatures $T>J$. CsNiCl_3 has an exchange interaction J that makes it an ideal system for studying high-temperature fluctuations, not only because the whole magnetic excitation spectrum can be measured with thermal neutrons but also because temperatures between J and $\sim 10J$ (room temperature) can readily be accessed.

Section II of the paper describes magnetic properties of CsNiCl_3 and gives the configuration of the neutron scattering spectrometers. Section III gives a thorough analysis of the measurements presented earlier.²² The inelastic time-of-flight neutron scattering measurements of the excitation spectrum between $T=12$ and 50 K are reported in Sec. IV. In this temperature range, resonant and dispersive excitations were observed for a wide range of wave-vector transfers along the chain. In Sec. V, we describe the measurement of the dynamic structure factor $S(\mathbf{Q},\omega)$ of the paramagnetic scattering at $T=200\text{ K}$. The results are summarized, discussed and put into an overall context in Sec. VI.

II. EXPERIMENTAL DETAILS

CsNiCl_3 is one of the best examples of a gapped weakly coupled spin-1 chain system. The crystal structure is hexagonal, D_{6h}^4 space group, with low-temperature lattice constants $a=7.14\text{ \AA}$ and $c=5.90\text{ \AA}$. The exchange interaction along the c axis $J=2.28\text{ meV}$ is much stronger²³ than the interaction in the basal plane $J'=0.044\text{ meV}$,^{6,21} making CsNiCl_3 a system of weakly coupled spin-1 chains. The Hamiltonian can be written as

$$\mathcal{H}=J\sum_i^{\text{chain}}\mathbf{S}_i\cdot\mathbf{S}_{i+1}+J'\sum_{\langle i,j\rangle}^{\text{plane}}\mathbf{S}_i\cdot\mathbf{S}_j-D\sum_i(S_i^z)^2. \quad (1)$$

The weak Ising anisotropy $D=4\text{ }\mu\text{eV}$ (Ref. 24) is small enough that CsNiCl_3 is a good example of an isotropic Heisenberg antiferromagnet.

Because of the interchain couplings CsNiCl_3 orders antiferromagnetically below $T_N=4.84\text{ K}$.²¹ Above T_N , CsNiCl_3 displays the characteristics of an isolated antiferromagnetic spin-1 chain: the excitation spectrum exhibits the Haldane gap, the correlations fall off exponentially and the magnetic susceptibility shows a broad maximum near 30 K .²⁵

The single crystal of CsNiCl_3 $5\text{ mm}\times 5\text{ mm}\times 20\text{ mm}$ was sealed in an aluminum can containing helium gas to prevent absorption of water. The experiments were performed using the cold-neutron RITA triple axis spectrometer²⁶ at the DR3 reactor of the Risø National Laboratory, Denmark, and the chopper time-of-flight spectrometer MARI at the pulsed spallation source ISIS of the Rutherford Appleton Laboratory, United Kingdom.

For the experiment using the RITA spectrometer, the sample was mounted in a cryostat with its (hhl) crystallographic plane in the horizontal scattering plane of the neutron spectrometer, and the temperature was controlled to an accuracy of 0.1 K between 1.5 and 70 K . The energy of the neutrons from a cold source was selected by a vertically focusing pyrolytic graphite monochromator. A rotating velocity selector before the monochromator suppressed unwanted neutrons that would be Bragg reflected by its higher order planes. Supermirror guides with $n=3$ ($\theta_c=1.2^\circ$ at 4 \AA) were located before and after the monochromator, and the beam was 20 mm wide. The scattered beam was filtered through cooled beryllium, passed through a 50 mm wide 1° Soller collimator, and was analyzed by reflection from the central two blades of a seven-component flat pyrolytic graphite analyzer aligned so that each blade reflected the same energy of neutrons, 5 meV . The Soller geometry meant that the beam reflected by the analyzers was about 20 mm wide and located in the central 30 strips of a position sensitive detector. Because the detector was 120 pixels wide ($\sim 120\text{ mm}$) the side strips were used to estimate and subtract the temperature independent background. Turning of either analyzer or monochromator from their reflecting position confirmed that the side pixels gave a good representation of the background arriving at the center of the detector. With this arrangement the low-energy resolution was typically 0.26 meV [full width at half maximum (FWHM)] in energy. The longitudinal and transverse wave-vector width of the (002) peak was 0.01 and 0.016 (FWHM in reciprocal lattice units) and the calculated vertical resolution was 0.22 \AA^{-1} .

For the experiment using the MARI spectrometer the sample was oriented with its (hhl) plane in the vertical scattering plane, and the c axis was either parallel or perpendicular to the incident beam direction. The incident neutron energy was either 20 or 30 meV with the Fermi chopper spinning at 150 Hz . The energy resolution was then 0.35 or 0.4 meV , respectively, as determined from the FWHM of the quasielastic peak. In time-of-flight measurements the energy resolution improves with increasing energy transfer and in our measurements the width of a resolution limited peak decreases by 25% from 0 to 6 meV energy transfer. Since this change is always less than 10% of the observed magnetic excitation width, the energy resolution at finite energy transfer was approximated by the quasielastic resolution. The FWHM resolution in the wave vector at zero energy transfer

was typically 0.02 \AA^{-1} along both the c^* and the $[110]$ directions and as large as 0.19 \AA^{-1} perpendicular to the scattering plane if only the central detector bank was used. The wave-vector resolution improved with increasing energy transfer. The measurements were performed with the sample at temperatures between $T=6.2$ and 200 K. The scattering was measured for a total proton charge between 4000 and $8600 \mu\text{Ah}$ at an average proton current of $170 \mu\text{A}$.

MARI has three detector banks two of which are out of the vertical scattering plane. For $T \leq 25$ K only data recorded by the central detector bank was included in the analysis because the two side banks sample an out-of-plane wave-vector transfer where the neutron scattering is different. All three detector banks were used for the measurements performed at temperatures $T \geq 50$ K where the 3D dispersion is small and good resolution perpendicular to the scattering plane is unnecessary.

III. EXPERIMENTAL RESULTS

A. Excitation at $Q_c=1$

Close to the antiferromagnetic point, denoted $Q_c=1$ because the spin spacing is $c/2$ along the chain, the excitation spectrum of an antiferromagnetic spin-1 chain in its quantum-disordered phase is dominated by well-defined, gapped spin-1 excitations (Haldane excitations) which satisfy a relativistic dispersion relation. We showed in a recent publication²² that for $T \leq \Delta$, the Haldane excitation at $Q_c=1$ exhibited a Lorentzian spectral form. We showed that its lifetime agrees well with a semiclassical theory²⁷ for gapped systems provided we replaced the classical dispersion by the more accurate relativistic dispersion of the NLSM. At higher temperatures the Haldane excitation evolves into a broad resonant feature. In this paper a more detailed analysis of the data is presented and results based on two different spectral functions are presented for temperatures between $T=5$ and $T=70$ K $\approx 2.7J$.

The Haldane excitation was measured at $\mathbf{Q} = (0.81, 0.81, 1)$ where the Fourier transform of the inter-chain coupling vanishes, and within a random phase approximation (RPA) the chains behave as if they were uncoupled.⁶ In Fig. 1, the results are shown at $T=6$ and 9 K. The spectra were fitted to both an antisymmetrized Lorentzian and an antisymmetrized Gaussian line shape, weighted by the Bose factor, and convoluted with the resolution function.²⁸ It is clear from the spectrum at $T=6$ K that an intrinsic Lorentzian line shape gives a better description of the measured data, as predicted by Damle and Sachdev.²⁷

The Lorentzian fits were performed with a double Lorentzian form, namely,

$$S(\mathbf{Q}, \omega) = A[n(\omega) + 1] \times \left(\frac{\Gamma}{[\omega - \epsilon(\mathbf{Q})]^2 + \Gamma^2} - \frac{\Gamma}{[\omega + \epsilon(\mathbf{Q})]^2 + \Gamma^2} \right), \quad (2)$$

where ω is the energy transfer and the Bose factor is defined by

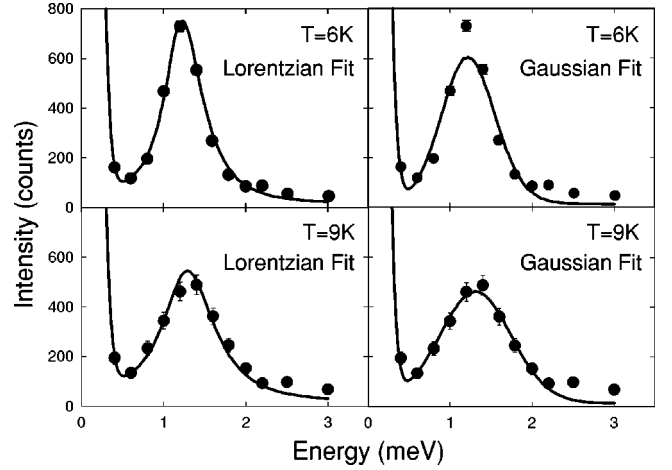


FIG. 1. Scattering from the Haldane excitation at $\mathbf{Q} = (0.81, 0.81, 1)$ for $T=6$ and 9 K as a function of energy transfer. The data were measured using the triple-axis spectrometer RITA as described in the text. The intensity was fitted to a Lorentzian (left) and a Gaussian (right) cross section convoluted with the resolution function (Ref. 28).

$$n(\omega) + 1 = \left[1 - \exp\left(-\frac{\hbar\omega}{k_B T}\right) \right]^{-1}. \quad (3)$$

The energy width is given by Γ (half Lorentzian width at half maximum) and the energy of the excitations by $\epsilon(\mathbf{Q})$. A is an overall scaling factor which scales as $1/\epsilon(\mathbf{Q})$ for antiferromagnetic spin waves and also for the excitations of the NLSM. With increasing temperature, the excitation broadens as may be seen at $T=9$ K, where the line shape can be described equally well by a Gaussian or Lorentzian line shape.

Another spectral form that describes damped excitations is the damped harmonic oscillator (DHO) function which can be written as

$$S(\mathbf{Q}, \omega) = \frac{A[n(\omega) + 1]4\Gamma\epsilon(\mathbf{Q})\omega}{[\omega^2 - \epsilon_{\text{DHO}}(\mathbf{Q})^2]^2 + 4\Gamma^2\omega^2}. \quad (4)$$

$\epsilon_{\text{DHO}}(\mathbf{Q})$ is the DHO energy and the other symbols are as in Eq. (2). The DHO function is the same function as the antisymmetrized Lorentzian defined in Eq. (2) if

$$\epsilon_{\text{DHO}}(\mathbf{Q})^2 = \epsilon(\mathbf{Q})^2 + \Gamma^2. \quad (5)$$

For the same spectral distribution, the DHO energy $\epsilon_{\text{DHO}}(\mathbf{Q})$ is therefore larger than the Lorentzian energy $\epsilon(\mathbf{Q})$.

In Fig. 2 we show that neutron scattering at $\mathbf{Q} = (0.81, 0.81, 1)$ at $T=25$ and 50 K is well described by a Lorentzian cross-section. The background was assumed to be constant and a Gaussian was used to account for the incoherent elastic scattering. The cross section [Eq. (2)], folded with the resolution function,²⁸ was fitted to the data to derive $\epsilon(\mathbf{Q})$, Γ and A .

The excitation energy $\epsilon(\mathbf{Q})$ and width Γ are shown in Figs. 3 and 4 as a function of temperature T . The Haldane gap energy, which at $T=5$ K is 1.2 meV, increases rapidly between $T=12$ and 30 K as the excitation develops into a

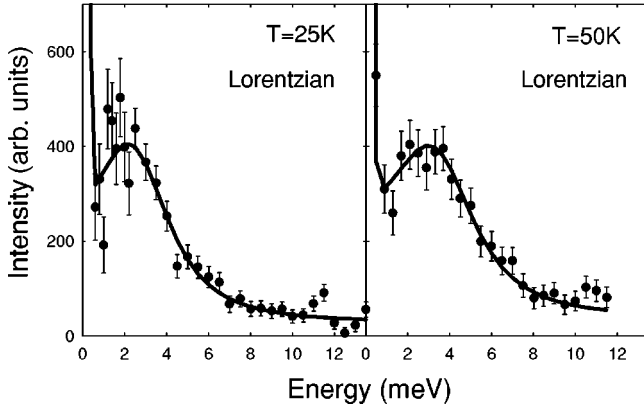


FIG. 2. Neutron scattering intensity at $\mathbf{Q}=(0.81, 0.81, 1)$ at $T=25$ and 50 K measured using RITA. The data is shown as a function of neutron energy transfer. The solid lines correspond to a Lorentzian cross section convoluted with the resolution ellipsoid and fitted to the data.

broad resonant feature. At about 30 K, a temperature of the order of the exchange coupling J along the chain, there is a crossover to a qualitatively different behavior and for $T > 30$ K the energy increases only slowly with increasing temperature.

The observed gap energies are compared in Fig. 3 (solid line) with the theory of Jolicœur *et al.*²⁹ based on the NL σ M, calculated with the $T=0$ K gap energy of $\Delta_0 = 10.6$ K we obtain from the exchange constant as $\Delta_0 = 0.406J$. The gap equation of NL σ M is a statement that

$$g \int_0^\infty dq \frac{2n(\epsilon_q) + 1}{\epsilon_q} = 1 \quad (6)$$

is a constant in temperature where

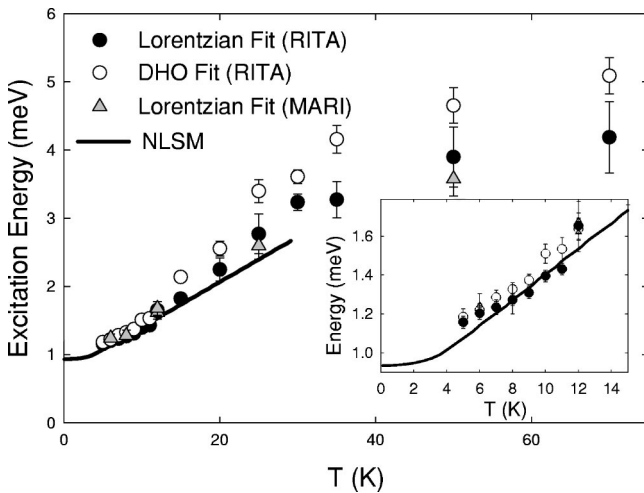


FIG. 3. Excitation energy $\epsilon(\mathbf{Q})$ for $\mathbf{Q}=(0.81, 0.81, 1)$ as a function of temperature between $T=5$ and 70 K. The energies were obtained from fits to a resolution-folded Lorentzian or damped harmonic oscillator function. The solid line shows the upward renormalization of the gap energy obtained from the NL σ M (Ref. 29). The inset shows the low-temperature range where NL σ M is valid.

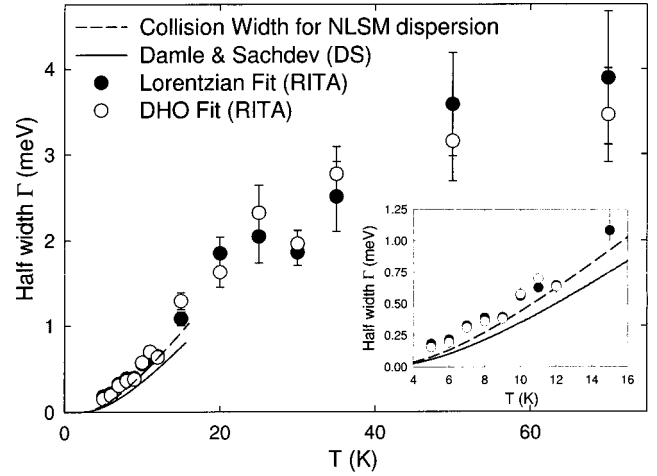


FIG. 4. Half width Γ , corrected for resolution, for $\mathbf{Q}=(0.81, 0.81, 1)$ between $T=5$ and 70 K. The widths were obtained from fits to a Lorentzian or a DHO function. The solid line is the prediction of Damle and Sachdev. The dashed line is our calculation of the free-particle collision width for the NL σ M dispersion. The inset shows the low-temperature range up to $T=15$ K where the NL σ M is valid.

$$\epsilon(q) = \sqrt{\Delta(T)^2 + v_s^2 q^2}. \quad (7)$$

This implicit equation for $\Delta(T)$ can be used to calculate the gap relative to Δ_0 which we take from experiment and use to obtain g at $T=0$ K. For $T < \Delta = 11$ K (see inset), where the theory is expected to be valid, the observed energy matches the theoretical prediction except below 7 K where the gap energy is higher. The good agreement for $7 \text{ K} < T < 11$ K shows that the NL σ M gives a good description of the low-temperature quantum-disordered phase for $T < \Delta$. The disagreement below $T < 7$ K is likely due to 3D interactions.³⁰ These give rise to low-energy modes as T_N is approached whose thermal population will drive up the gap energy in the NL σ M equation [Eq. (6)].

The measured widths Γ are shown in Fig. 4. The width is always smaller than the excitation energy up to at least $T=70$ K because the upward renormalization of the excitation energy is fast enough to overcome the increasing damping. Damle and Sachdev²⁷ have developed a theory of the damping of excitations in gapped spin systems which is valid as long $T < \Delta$. In CsNiCl₃ this temperature range is limited because $\Delta = 0.41J = 11$ K and 3D effects are important close to the ordering temperature T_N . As shown in Fig. 4 their theory, which approximates the NL σ M dispersion by a classical form, $\Delta + v_s^2 q^2 / 2\Delta$, predicts considerably longer excitation lifetimes than those observed experimentally. However, we find that a larger half-width arises when we calculate the collision time for the density and root mean square relative velocity of particles that move freely according to the elementary excitation particles by the more accurate relativistic dispersion of the NL σ M [Eq. (7)]. Details of our calculations are given in Sec. VA. Below $T=8$ K, the observed width is consistently higher than that predicted by the theory. Probably this is due to the 3D spin correlations which are most important close to T_N . The wave vector \mathbf{Q}

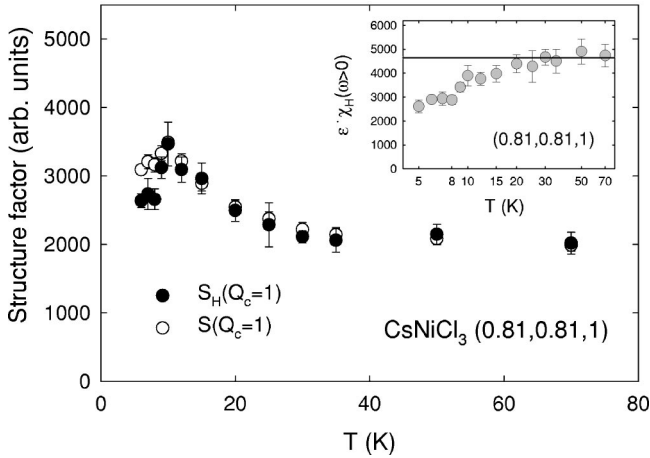


FIG. 5. Structure factor at the 1D point $\mathbf{Q}=(0.81, 0.81, 1)$ as a function of temperatures. The solid circles show the integrated intensity of the Haldane excitation $S_H(\mathbf{Q})$. The open circles represent $S(\mathbf{Q})$ determined from the entire neutron scattering intensity. Inset: The susceptibility of the Haldane excitations for positive energy transfer, defined as $\chi_H(\mathbf{Q}) = \int_0^\infty d\omega S_H(\mathbf{Q}, \omega) / \{n[\epsilon(\mathbf{Q})] + 1\}$, multiplied with the excitation energy $\epsilon(\mathbf{Q})$ shows a transition to a qualitatively different behavior at ~ 15 K.

$= (0.81, 0.81, Q_c)$ is the one-dimensional wave vector with regard to the energy dispersion, but other properties such as the linewidth will be influenced by 3D interactions. We expect that the exponentially greater thermal population of the low-lying 3D gap modes will shorten the collision lifetime relative to that for the gap of an isolated chain.

Above about $T=20$ K $\sim J$ the temperature dependence of the excitation width decreases, similar to that of the energy. This behavior probably arises because the lattice momentum cutoff is not properly included in the theoretical model. The cutoff is infinite in Ref. 27, and in our relativistic calculation it was limited to $q = \pi$ (see Sec. VA). An extension of the theory to higher temperatures would be valuable.

Our results cannot be directly compared to measurements by Zaliznyak *et al.*,¹³ because they probed the spin dynamics close to the ordering wave-vector. When the system orders one expects that the system collects intensity in a narrow region near the ordering wave vector, and consequently, their results are strongly influenced by 3D interactions.

Figure 5 shows the integrated intensity of the Haldane excitation $S_H(\mathbf{Q})$, for $\mathbf{Q}=(0.81, 0.81, 1)$, the 1D point, as a function of temperature (solid circles). The S_H was determined from the observed neutron scattering intensity by integrating the area under the Lorentzian cross section for positive and negative energies. It includes all the scattering except below ~ 12 K where the spectrum contains a high energy continuum of 12(2)% in weight.³¹ S_H increases with decreasing temperature as the antiferromagnetic fluctuations become stronger and the spectral weight is displaced to lower energy. The increase between $T=50$ and 20 K is associated with the growth of the 1D correlation length. However, at 10 K the temperature dependence of S_H has a peak and then decreases with decreasing temperature. This is correlated with the holdup in the gap decrease noted for Fig. 3.

The structure factor $S(\mathbf{Q})$ for $\mathbf{Q}=(0.81, 0.81, 1)$, which

includes the continuum, has a lesser decrease at low temperatures (Fig. 5). $S(\mathbf{Q})$ was determined by numerical integration of the observed neutron spectrum at positive energy transfers and adding intensity at negative energy transfer calculated using the detailed balance relation. $S(\mathbf{Q})$ and $S_H(\mathbf{Q})$ are identical at high temperatures, but for $T < 10$ K, where the continuum scattering was observed, $S(\mathbf{Q})$ is larger than $S_H(\mathbf{Q})$ and approximately constant. The increase in $S(\mathbf{Q})$ on cooling is substantially less than that calculated for isolated chains.³²

To test whether the spectral weight scales with $1/\epsilon(\mathbf{Q})$ we divided S_H by the population factor $n[\epsilon(\mathbf{Q})] + 1$ to obtain the susceptibility for positive energy transfer χ_H and multiplied it with the excitation energy $\epsilon(\mathbf{Q})$. This approximately removes the thermal factor to a degree that improves as the temperature and width decrease. Our scaled function (Fig. 5) is a constant for $T > 15$ K, showing that the intensity scales with $1/\epsilon(\mathbf{Q})$. For $T < 15$ K, however, χ_H is lower than expected from a $1/\epsilon(\mathbf{Q})$ dependence of the intensity, thus the spectral weight grows more slowly than $1/\epsilon(\mathbf{Q})$.

The reason for the behavior below $T=10$ K is at present unclear. In Kenzelmann *et al.*³¹ we have argued that the continuum scattering is generated by the interchain coupling which has a strong effect on the dispersion for temperatures close to the ordering temperature T_N despite its small size. As will be shown in a forthcoming publication³³ the interchain coupling has a strong effect on the excitation intensity for all temperatures $T < 50$ K and there is considerably less magnetic intensity in $S_H(\mathbf{Q})$ as well as in $S(\mathbf{Q})$ near $Q_c = 1$ than in uncoupled chains. We may also imagine as T_N is approached that spectral weight is transferred from the 1D point to the 3D ordering wave vector.

B. The dispersion relation

The spectrum of excitations of CsNiCl_3 was measured for $T=12, 25,$ and 50 K over a wide range of wave-vector transfers using the MARI spectrometer with the incident beam perpendicular to the c axis. The neutron scattering was measured for energy transfers of up to 75% of the incident energy. For a 1D magnet, the scattering $S(\mathbf{Q}, \omega)$ was obtained as a function of Q_c and ω , where Q_c is the component of the wave-vector transfer along the chain, while the in-plane wave-vector Q_a is a known function of Q_c and of the energy transfer.

For measurements below $T \leq 25$ K, where the excitations may exhibit a dispersion perpendicular to the chain direction, only data from the central detector banks were taken to limit the out-of-plane wave vectors sampled in the experiment. Figures 6 and 7 show the observed neutron scattering intensity for three wave-vector transfers along the chain at $T=25$ and 50 K. With increasing temperature, the intensity for $Q_c=1$ decreases, moves to higher energies and broadens, as discussed in the previous section.

Our previous study has shown that the excitation at $Q_c = 1$ remained resonant up to 70 K.²² Figures 6 and 7 further show that the excitations remain resonant throughout the zone and that they are weakly dispersive even at 50 K. The scattering was again fitted to the Lorentzian of Eq. (2) but

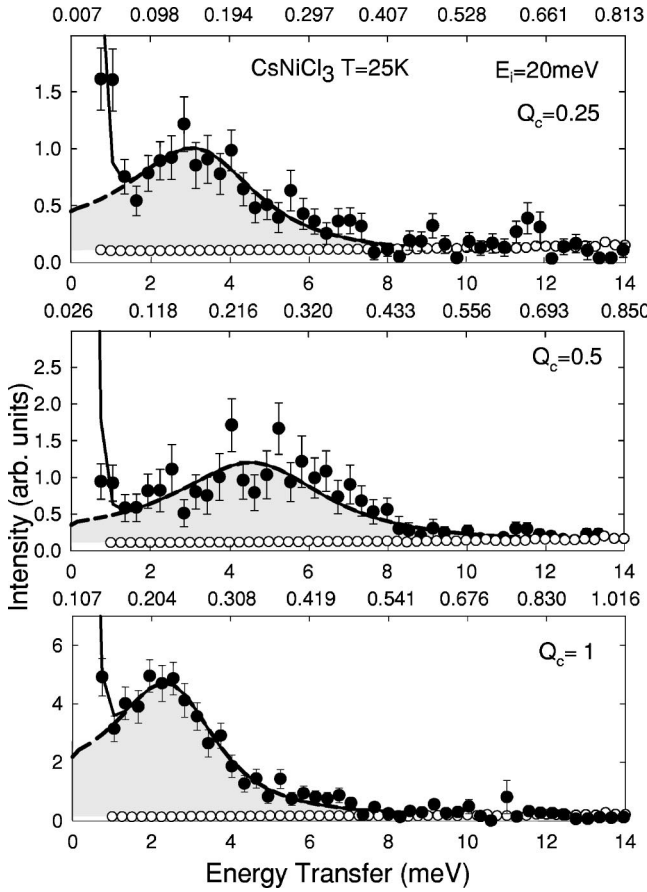


FIG. 6. Time-of-flight neutron scattering spectra at $T=25$ K for three different Q_c . The $Q_{[110]}$ wave-vector dependence is shown on the top axes of the graphs. For $Q_c=1$ only data from the central detector bank is shown, for $Q_c=0.5$ and $Q_c=0.25$ data from the three detector banks was found to be indistinguishable and was added for this graph. The solid line is the antisymmetrized Lorentzian weighted with the Bose factor and a quasielastic peak describing the incoherent scattering. Shaded areas correspond to magnetic scattering only and open circles show the background as explained in the text.

now taking the line shape of the quasielastic peak for the energy resolution. Least-square fits gave the parameters of Eq. (2), A , $\epsilon(\mathbf{Q})$, and Γ (see in Fig. 8). Data with $Q_c > 1.3$ was not analyzed because they were contaminated with phonon scattering.

The nonmagnetic background was estimated from the scattering observed in detectors at high scattering angles where the wave-vector transfer $|\mathbf{Q}|$ is large, the magnetic form factor is low and the spectrum is dominated by the phonon scattering which is proportional to $|\mathbf{Q}|^2$. The nonmagnetic background for each scan was obtained by scaling the intensity according to $|\mathbf{Q}|^2$ and accounting for background scattering that is independent of $|\mathbf{Q}|$. The latter was estimated from the energy gain side of the spectrum at low temperatures. The background is shown in Figs. 6 and 7 by open circles. Assuming that the whole intensity at high scattering angle scales only with $|\mathbf{Q}|^2$, or that part of the scattering scales with $|\mathbf{Q}|^4$ leads to even lower background estimates for the low-angle data. The results show that the

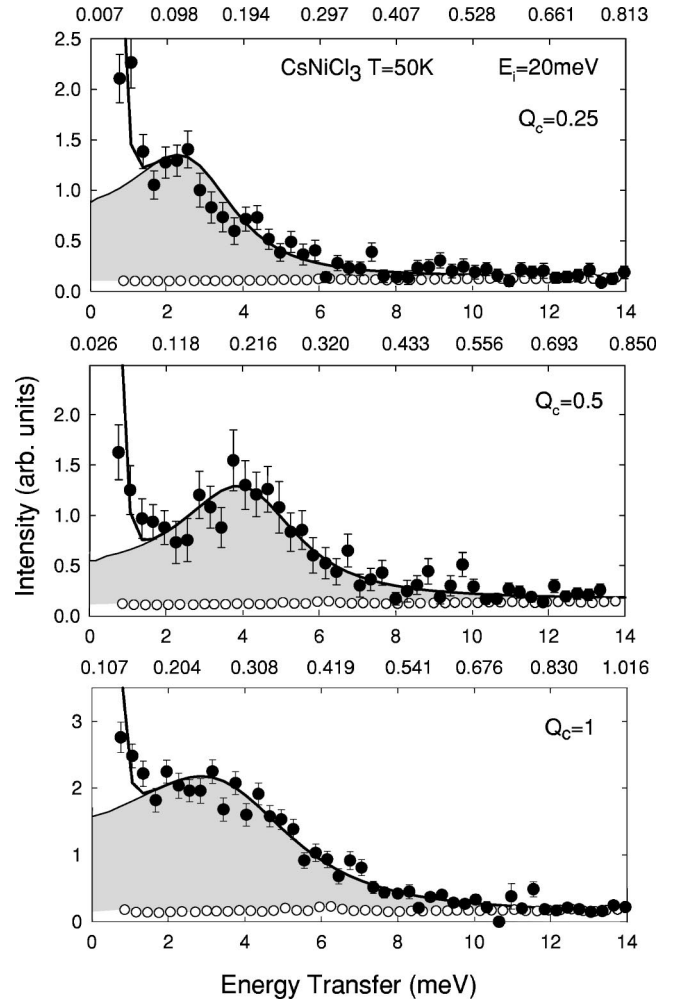


FIG. 7. Time-of-flight neutron scattering spectra at $T=50$ K for three different Q_c . The $Q_{[110]}$ wave-vector dependence is shown on the top axes of the graphs. The solid line is the antisymmetrized Lorentzian weighted with the Bose factor and a quasielastic peak describing the incoherent scattering. Shaded areas correspond to magnetic scattering only and open circles show the background as explained in the text.

background is weakly dependent on energy transfer and therefore may be accurately subtracted.

The dispersion of the excitations decreases with increasing temperature as shown in Fig. 8(a). While the excitation energy increases with increasing temperature for antiferromagnetic fluctuations, it decreases for $Q_c=0.25$ and 0.5 . Due to the lack of a theoretical model for the dynamic structure factor for the whole magnetic zone the dispersion was phenomenologically described by

$$\omega^2(Q_c, T) = \Delta^2(T) + v_s^2(T) \sin^2(\pi Q_c) + \alpha^2(T) \cos^2(\pi Q_c/2). \quad (8)$$

Here $\Delta(T)$ is the Haldane gap at $Q_c=1$, $v_s(T)$ is the spin velocity determining the increase of the excitation energy as $|Q_c-1|$ increases, and $\alpha(T)$ takes account of the two-particle peak at low T as $Q_c \rightarrow 0$, but in practice α is used as a free parameter to account for the asymmetry about $Q_c=0.5$. For $T \leq 25$ K 3D effects were taken into account using

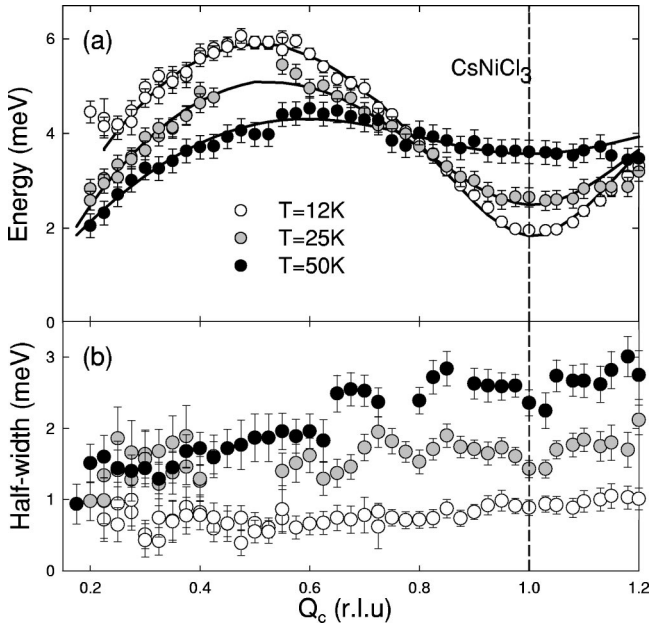


FIG. 8. (a) Excitation energy $\epsilon(Q_c)$ as a function of wave vector and temperature. The lines are fits described in the text. (b) Lorentzian half width Γ .

a RPA approximation which introduces a small dispersion perpendicular to the chain axis.³⁴ The dispersion then reads

$$\omega^2(\mathbf{Q}) = \omega(Q_c)[\omega(Q_c) + 2J'(Q_a, Q_b, 0)S(\mathbf{Q})], \quad (9)$$

where $J'(Q_a, Q_b, 0)$ is the Fourier transform of the interchain coupling and $S(\mathbf{Q}) = \int S(\mathbf{Q}, \omega) d\omega$ is the structure factor. The dispersion perpendicular to the chain is most pronounced at $Q_c = 1$, where $S(\mathbf{Q})$ is maximum and is small at $Q_c = 0.5$.

The Haldane gap or resonance energy Δ , the spin velocity v_s and α were obtained for the different temperatures by fitting Eq. (9) to the \mathbf{Q} dependence of the excitation energies. The interchain coupling J' was kept fixed in the fits because the scattering shows a 3D dependence for $T < 50$ K.³⁵ The results for $\Delta(T)$ are shown in Figs. 3(a) and 8 and are consistent with previous results.²² The results for $v_s(T)$ and $\alpha^2(T)$ are shown in Fig. 9. The spin velocity v_s is approximately constant below 15 K at 5.70(7) meV and above 15 K it decreases with temperature reaching 3.4(1) meV at 50 K. The asymmetry parameter α^2 is 6 meV² at $T = 6$ K, decreases rapidly with increasing temperature and becomes negative above about 12 K. Since it is merely a phenomenological parameter, this is not unphysical but reflects the reversal of the asymmetry about $Q_c = 0.5$ as the high temperature limit is approached.

The excitations strongly broaden with increasing temperature [Fig. 8(b)]. Below $T = 25$ K, the width is approximately independent of the wave vector. For $Q_c > 1.2$ the width begins to increase and we have evidence that the scattering there is contaminated with phonons and so these data were not further analyzed. For $T = 50$ K the excitation width increases from $Q_c = 0.2$ to $Q_c = 1$ —an indication of a change in its Q_c dependence with increasing temperature. We shall

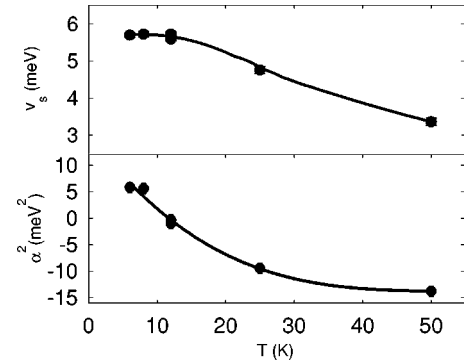


FIG. 9. The upper panel shows the spin velocity v_s and the lower panel α^2 as a function of temperature. The solid lines are guides to the eye.

see that this is expected at high temperatures. The widths shown in Fig. 8(b) are slightly smaller relative to those in Fig. 4, presumably because the resolution width was overestimated in our analysis.

C. Structure factor and correlation length

The structure factor $S(\mathbf{Q})$ was determined numerically from the measured neutron spectra at positive energy transfer after subtraction of the flat background. The intensity at negative energy transfers was estimated using detailed balance. The structure factor was corrected for the wave-vector dependence of the magnetic form factor and for the effect of the 3D interactions by using Eq. (9) to derive the structure factor for the fluctuations at the 1D point

$$S(Q_c) = \frac{\omega(\mathbf{Q})}{\omega(Q_c)} S(\mathbf{Q}). \quad (10)$$

This can be thought of as the structure factor of a single chain embedded in the system.

The effective structure factor for the 1D chain (Fig. 10) shows strong antiferromagnetic fluctuations at $Q_c = 1$ that persist to $T \sim 2J$. They decline with temperature while $S(Q_c)$ at $Q_c = 0.25$ and 0.5 increases. For a 1D magnet with a magnetic excitation spectrum that is dominated by a single mode, the Q_c dependence of the structure factor $S^{\alpha\alpha}(Q_c)$, $\alpha = x, y, z$, can be expressed as³⁶

$$S^{\alpha\alpha}(Q_c) = -\frac{4}{3} \frac{\langle \mathcal{H} \rangle}{L} \frac{(1 - \cos \pi Q_c)}{\hbar \omega^{\alpha\alpha}(Q_c)}. \quad (11)$$

Here $\langle \mathcal{H} \rangle / L$ is the ground state energy per spin and $\omega^{\alpha\alpha}(Q_c)$ is the single mode energy. This approximation is called the single mode approximation (SMA). Taking the energy from Eq. (8), the structure factor close to the antiferromagnetic point behaves as a square-root Lorentzian

$$S(Q_c) \propto \frac{\xi}{\sqrt{1 + \pi^2(Q_c - 1)^2 \xi^2}}, \quad (12)$$

where we expect

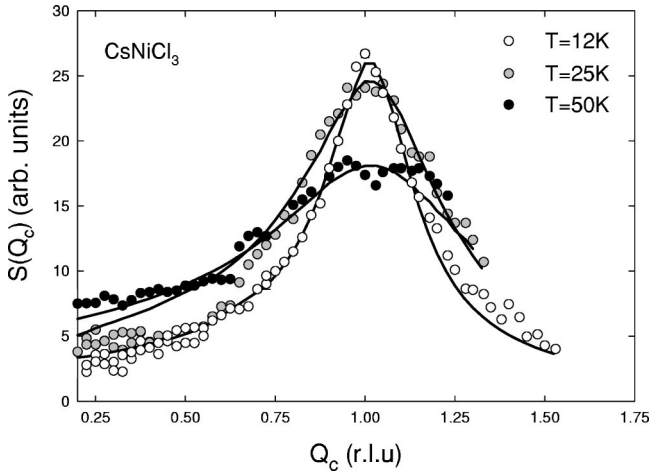


FIG. 10. Structure factor $S(Q_c)$ along $(0.81, 0.81, Q_c)$ for $T = 12, 25,$ and 50 K after an allowance for 3D effects [Eq. (10)]. $S(Q_c)$ was corrected for background and magnetic form factor. The solid lines correspond to a fit to a square-root Lorentzian [Eq. (12)] as explained in the text.

$$\xi = \frac{\sqrt{v_s^2 + \alpha^2/4}}{\Delta}, \quad (13)$$

and where ξ is the correlation length. ξ was determined from $S(Q_c)$ for $0.7 < Q_c < 1.3$ by fitting Eq. (12) to the data shown in Fig. 10.

The temperature dependence of the correlation length ξ is shown in Fig. 11 on a semilogarithmic plot. At 50 K it is only slightly longer than 1 site which means that the spatial correlations are extremely short ranged. It is surprising to have resonant and dispersive modes in a spin system with such a short correlation length. With decreasing temperature, the correlation length increases to about 4 sites below 8 K, as previously reported.³⁰ These results can be compared to the correlation length obtained by Kim *et al.*³² from numerical quantum Monte Carlo calculations in which effective

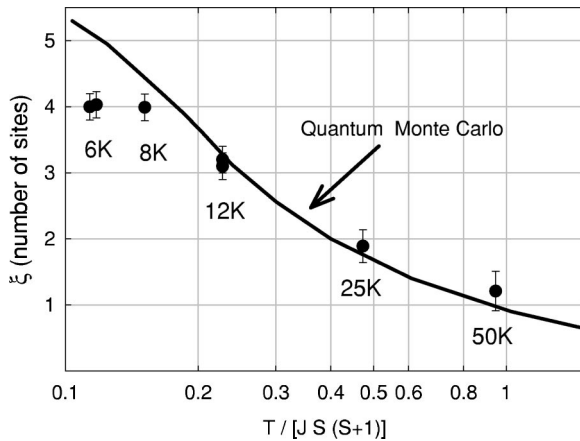


FIG. 11. Correlation length $\xi(T)$ deduced from $S(Q_c)$ and shown as a function of the reduced temperature $T/[JS(S+1)]$ on a semilogarithmic plot. The solid line is the prediction of the correlation length obtained from a quantum Monte Carlo calculation (Ref. 32) for an $S=1$ chain.

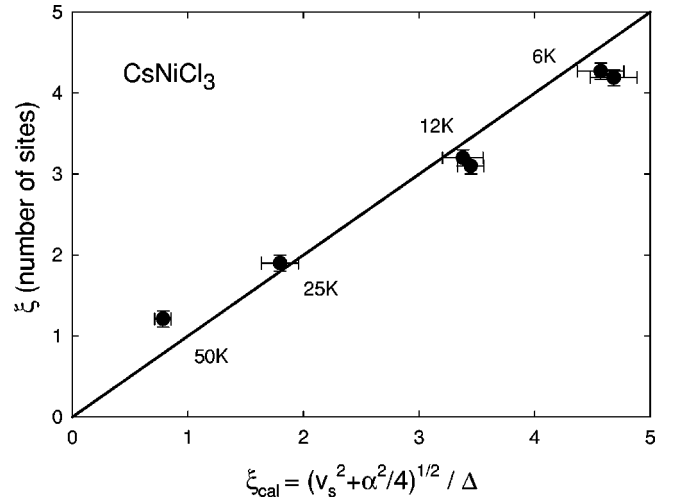


FIG. 12. The horizontal axis represents the correlation length ξ_{cal} calculated from the experimentally determined Δ , v_s , and α for temperatures between $T=6$ and 50 K. The vertical axis shows the correlation length ξ determined from the wave-vector dependence of the structure factor $S(Q_c)$. The solid line is $\xi_{\text{cal}} = \xi$.

spin S chains were realized by ferromagnetically coupling $n=2S$ antiferromagnetic spin chains with $S=1/2$.³² Our measured correlation length for temperatures above 12 K is in excellent agreement with the numerical results, and only below 12 K where 3D correlations are most important is the correlation length shorter than the numerical prediction for uncoupled spin-1 chains. That it becomes shorter is associated with the fact that we are at the noncritical 1D wavevector.

For a 1D magnet in which the magnetic response is dominated by single mode excitations, the SMA [Eq. (8)] predicts that ξ is given by Eq. (13). In this experiment, all four quantities were independently determined and the relationship can be tested experimentally. Figure 12 compares the correlation length ξ estimated from the Q_c dependence of the structure factor and the correlation length ξ_{calc} given by Eq. (13). The agreement is excellent for all temperatures. This demonstrates that SMA is valid up to $T=50$ K and suggests that the observed excitations can be regarded as short-lived single particle excitations.

The Hohenberg-Brinkman sum rule³⁶ predicts that the first energy moment $F(Q) = \int_{-\infty}^{\infty} d\omega \omega S(Q, \omega)$ of a 1D magnet with isotropic nearest-neighbor exchange J is given by

$$F(Q_c) = -\frac{4}{3} \frac{\langle \mathcal{H} \rangle}{L} (1 - \cos(\pi Q_c)). \quad (14)$$

Here Q_c is the wave-vector transfer along the spin chain and $\langle \mathcal{H} \rangle = 3J \sum_i \langle S_i^\alpha S_{i+1}^\alpha \rangle$ is the expectation value of the Hamiltonian.

The first energy moment $F(Q_c)$ was determined numerically from the measured neutron scattering spectrum after subtraction of the background and accounting for the magnetic form factor, and is shown in Fig. 13 for three different temperatures. The dependence on Q_c of the first moment $F(Q_c)$ is in excellent agreement with the sum rule for all momenta and temperatures. The fit yields the internal energy

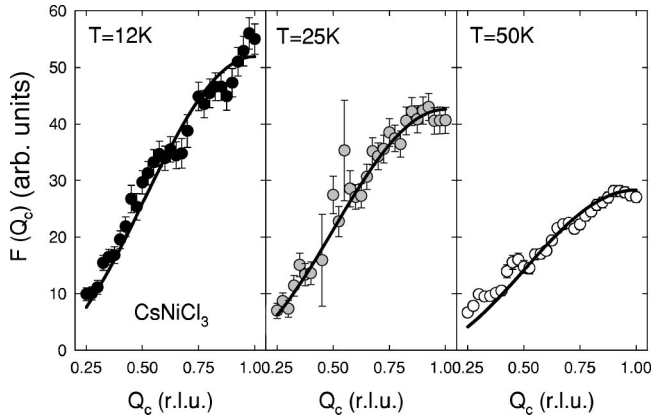


FIG. 13. First energy moment $F(Q_c) = \int_{-\infty}^{\infty} d\omega \omega S(Q, \omega)$ for $T = 12, 25,$ and 50 K. The solid line is a fit of the Hohenberg-Brinkman sum rule [Eq. (14)] to a parameter proportional to the internal energy $\langle \mathcal{H} \rangle$ (Ref. 36).

$\langle \mathcal{H} \rangle$ in arbitrary units and its temperature dependence, and it will be discussed in a forthcoming publication.³³ The data for $\langle \mathcal{H} \rangle$ are shown in Table I.

IV. HIGH-TEMPERATURE PARAMAGNETIC SCATTERING

At infinite temperature, there are no correlations between the spins and the instantaneous structure factor $S(\mathbf{Q})$ is a constant. The first moment of the spectrum vanishes for all \mathbf{Q} because the Bose factor weighs the excitations for neutron energy gain and loss equally. The second moment, however, is predicted to vanish at ferromagnetic momenta and reach a maximum at antiferromagnetic momenta, irrespective of the spin quantum number or whether the exchange is antiferromagnetic or ferromagnetic.^{37,38} Chain systems with nearest-

TABLE I. For neutron energy loss, the integrated intensity $R_0(\mathbf{Q}) = \int_0^\infty d\omega S(\mathbf{Q}, \omega)$ and the first and second moment $\langle \omega \rangle(\mathbf{Q}) = \int_0^\infty d\omega S(\mathbf{Q}, \omega) \omega / R_0(\mathbf{Q})$ and $\langle \omega^2 \rangle(\mathbf{Q}) = \int_0^\infty d\omega S(\mathbf{Q}, \omega) \omega^2 / R_0(\mathbf{Q})$ of the observed spectra. R_0 is in arbitrary units (a.u.) and $\langle \omega \rangle$ and $\langle \omega^2 \rangle$ are in units of meV and meV², respectively. Columns 2 to 4 are derived from MARI data with a varying wave-vector transfer perpendicular to the chain. The final columns are derived from the RITA data with a different normalization.

T (K)	$Q_c=0.5$			$Q_c=1$			$\langle \mathcal{H} \rangle$ (a.u.)	$\mathbf{Q}=(0.81, 0.81, 1)$		
	R_0 (a.u.)	$\langle \omega \rangle$	$\langle \omega^2 \rangle$	R_0 (a.u.)	$\langle \omega \rangle$	$\langle \omega^2 \rangle$		R_0 (a.u.)	$\langle \omega \rangle$	$\langle \omega^2 \rangle$
6	6.1(0.9)	5.8(0.3)	6.0(0.3)	22.2(0.7)	2.6(0.1)	3.3(0.1)	-28(0.4)	1316(21)	1.76(0.05)	2.35(0.09)
7								1362(45)	1.96(0.1)	2.49(0.08)
8	5.2(1.1)	5.4(0.5)	5.6(0.4)	20.7(0.9)	2.57(0.17)	3.25(0.23)	-27(0.5)	1323(44)	2.06(0.08)	2.57(0.05)
9								1322(46)	1.91(0.12)	2.53(0.16)
10								1404(32)	1.95(0.06)	2.36(0.05)
12	4.3(1.0)	5.8(0.6)	5.9(0.4)	20.84(0.66)	2.89(0.6)	3.58(0.22)	-26(0.5)	1233(45)	2.17(0.13)	2.78(0.13)
15								1055(42)	2.17(0.16)	2.52(0.23)
20								939(39)	3.1(0.2)	3.62(0.13)
25	6.1(1.0)	5.0(0.4)	5.4(0.3)	16.55(0.48)	3.72(0.2)	4.37(0.24)	-21.3(0.2)	813(37)	3.04(0.22)	3.66(0.15)
30								729(36)	3.0(0.23)	3.48(0.18)
35								689(35)	3.37(0.25)	4.03(0.14)
50	5.3(0.9)	4.4(0.3)	4.9(0.3)	10.89(0.26)	4.03(0.12)	4.49(0.1)	-14.2(0.2)	641(29)	3.75(0.23)	4.43(0.09)
70								571(28)	3.78(0.26)	4.43(0.1)
200	5.2(0.9)	3.5(0.2)	4.0(0.2)	7.5(0.19)	4.46(0.14)	4.95(0.12)	-3.8(0.1)			

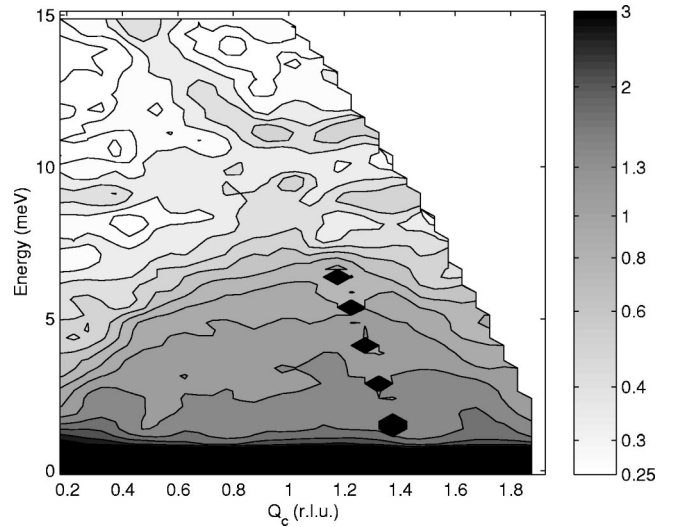


FIG. 14. The intensity measured at $T = 200$ K using MARI. The data were measured with an incident energy $E_i = 20$ meV and the intensity in all three detector banks was added and smoothed. The intensity is indicated by the bar on the right-hand side. The black trapezoidal areas are an artifact and a result of a MARI detector gap in the 2Θ scattering angle and the data smoothing algorithm. The quasielastic scattering below ~ 1 meV should be ignored.

neighbor interactions are ideal systems to test this behavior, because the wave-vector dependence of the second moment has a simple form

$$\langle \omega^2 \rangle \propto J^2 [1 - \cos(\pi Q_c)], \quad (15)$$

where Q_c is the wave-vector transfer along the chain.

The scattering was measured at $T = 200$ K $\approx 10J$ for a wide range of wave-vector transfers using the MARI spectrometer. Figure 14 shows the scattering surface projected

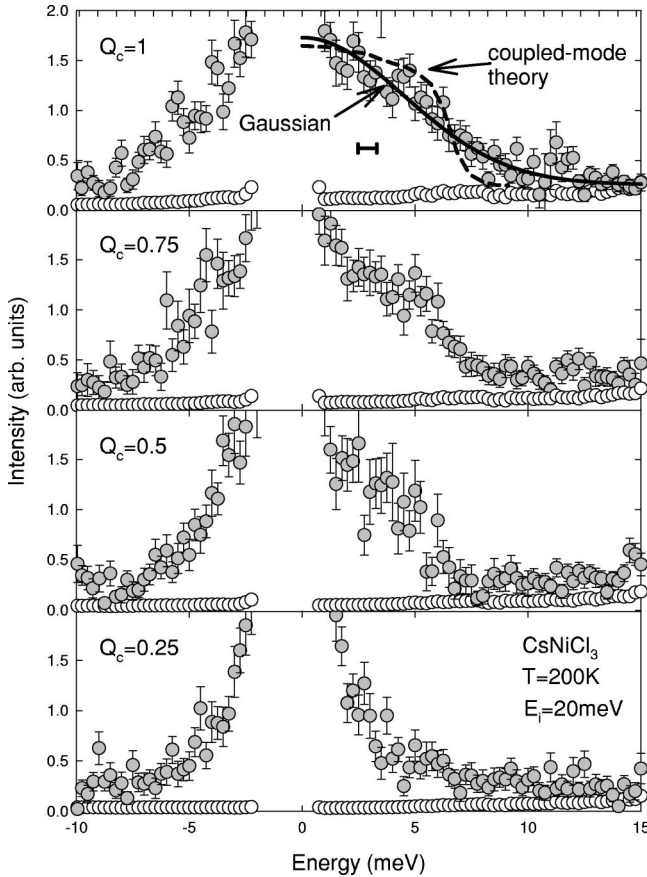


FIG. 15. Neutron spectra at $T=200$ K for four different Q_c . The peak centered at zero energy transfer arises from quasielastic incoherent scattering from the sample and the sample holder. The open circles show the background as explained in the text. The dashed and solid lines are the prediction of a coupled-mode theory at infinite temperature (Ref. 39) and the de-Gennes Gaussian (Ref. 37) fitted to the data, respectively. The instrumental resolution (FWHM) is shown by a bar.

onto the (Q_c, ω) plane for neutron energy loss. Because the effect of the interchain interaction is negligible at $T=200$ K, the data from all the detectors were used to improve the statistics. Figure 14 shows that the scattering consists of broad scattering and that there is no sign of the resonant excitations seen at lower temperatures. The broad dome of spectral weight is centered at $Q_c=1$ for the high energy fluctuations whereas it was located at $Q_c=0.5$ at low temperatures.

Figure 15 shows constant- Q_c scans for different wave vector. The upper bound of the scattering has a maximum of 10 meV at $Q_c=1$ and decreases with increasing $|Q_c-1|$.

The scattering intensity observed at the antiferromagnetic point $Q_c=1$ is not consistent with the prediction of a coupled-mode theory at infinite temperature,³⁹ shown as a dashed line in Fig. 15. Instead the scattering spectrum has the form of a Gaussian as predicted by de Gennes³⁷ (solid line). The difference between the coupled-mode theory and the experiment may be because the experiment was performed at a finite temperature but more likely because the theory is unsatisfactory.

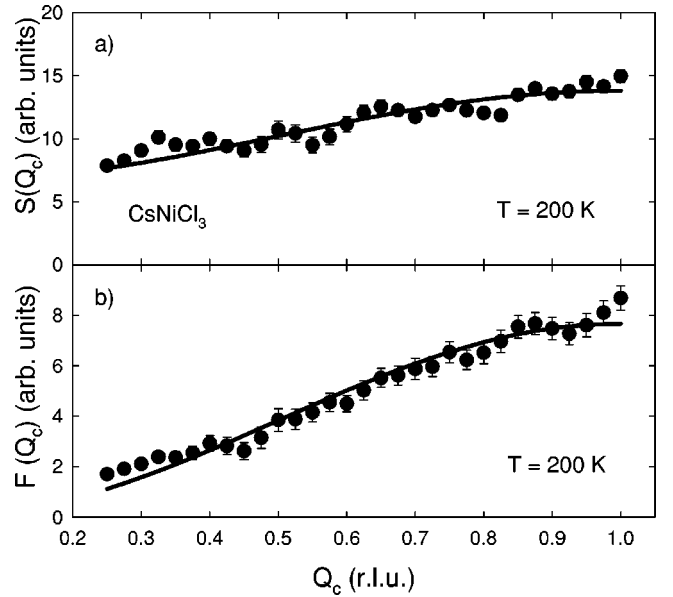


FIG. 16. (a) $S(Q_c)$ as a function of wave-vector transfer Q_c at $T=200$ K in the same units as in Fig. 10. The solid line is the prediction of the high-temperature series expansion [Eq. (28)] (Ref. 38), normalized to the data. (b) Observed first energy moment $F(Q_c)$. The solid line is the fit of the Hohenberg-Brinkman sum rule $-\frac{4}{3}(\langle \mathcal{H} \rangle / L)[1 - \cos(\pi Q_c)]$.

The structure factor $S(Q_c)$ and the first energy moment $F(Q_c)$ are shown in Fig. 16 in the same units as for the lower temperatures (Figs. 8 and 10). They were calculated numerically from the observed neutron scattering at positive neutron energy transfers after subtraction of a flat background that matched the scattering at high energy transfers. The intensity at negative energy transfers was estimated using detailed balance. $S(Q_c)$ and $F(Q_c)$ were corrected for the magnetic form factor. $S(Q_c=1)$ is now only about twice $S(Q_c=0.25)$, showing that there are weak spin correlations, which are considerably reduced compared to lower temperatures. The solid line is the prediction of a high-temperature series expansion [Eq. (28)] which will be discussed in Sec. V.

The Q_c dependence of the first moment $F(Q_c)$ is well described with the sum rule of Hohenberg and Brinkman,³⁶ confirming that the scattering is magnetic and that contamination with phonon scattering is not significant. The maximum of $F(Q_c)$ is ~ 6.5 times lower at 200 K than the maximum at 12 K, showing that although the first moment is not zero, the system is close to the high-temperature limit.

It is clear from Figs. 14 and 15 that the second moment has a maximum at the antiferromagnetic point $Q_c=1$ as predicted by the theory of de Gennes. It will be shown in the Sec. V that there is quantitative agreement between experiment and theory if the scattering is expanded to first order in $1/k_B T$.

V. DISCUSSION

A. Lifetime of Haldane excitation for $T < \Delta$

The excitations of an antiferromagnetic isolated spin-1 chain in its quantum-disordered phase are well defined,

gapped spin-1 excitations (Haldane excitations) which satisfy a relativistic dispersion relation $\epsilon(q) = (\Delta^2 + v_s^2 q^2)^{1/2}$, where $q = |Q - 1|$. At zero temperature where the spin correlation length is six sites,³² the neutron injects an excitation in the Haldane band which travels with a group velocity $v_s^2 q / \epsilon(q)$, and its lifetime is infinitely long. At a finite temperature $T \leq \Delta = 0.41J$, thermal activation creates a dilute gas of Haldane excitations. They limit the lifetime of the injected excitation through collisions, and this gives it a finite energy.²⁷

The scattering matrix for a two-particle collision has a superuniversal form in 1D which does not depend on any microscopic parameter, and for $T \ll \Delta$, it predicts that a two-particle state $(\{q_1, \sigma_1\}, \{q_2, \sigma_2\})$ transforms into a final state $(\{q_1, \sigma_2\}, \{q_2, \sigma_1\})$, where σ is the spin quantum number, thus basically swapping the spin.²⁷ Alternatively in 1D we may think that the particle created by the neutron, $\{q_1, \sigma_1\}$, collides with one of the gap particles $\{q_2, \sigma_2\}$ and, similar to billiard balls, the momentum of the first is transmitted to the second, to give $\{q_2, \sigma_1\}$ and $\{q_1, \sigma_2\}$. This result holds for any form of 1D dispersion relation. Damle and Sachdev²⁷ calculated the temperature dependence of the line shape and width by approximating the relativistic dispersion with a classical dispersion $\epsilon_{cl}(q) = \Delta + v_s^2 q^2 / 2\Delta$, and when $T \ll \Delta$, the dynamic structure factor has a simple scaling form

$$S(Q, \omega) = \frac{Ac}{\gamma\Delta} \Phi\left(\frac{\omega - \epsilon_{cl}(q)}{\gamma}\right), \quad (16)$$

where γ is the inverse of the time between collisions with other excitations and A is a scaling constant. The scaling function $\Phi(z)$ was calculated numerically and found to be close to the Lorentzian form

$$\Phi(z) = \frac{\pi\alpha}{2(\alpha^2 + z^2)}, \quad (17)$$

with $\alpha = 0.71$. Thus the DS theory predicts that the observed half-width is $\Gamma_{DS} = \alpha \cdot \gamma$. The inverse DS collision time is equal to the density of the excitations times their root mean square relative velocity, namely,

$$\gamma(T) = \frac{3k_B T \sqrt{2}}{\sqrt{2}\pi} \exp\left(-\frac{\Delta}{k_B T}\right), \quad (18)$$

the same as for classical gas collisions. The experimentally observed excitation Γ width in CsNiCl₃ is appreciably higher than this prediction as shown in Fig. 4 for all $T < \Delta \approx 11$ K.

We have performed our own calculations in which, as proposed by Damle and Sachdev, the excitations of a spin-1 chain at low temperatures are regarded as a dilute gas of particles whose lifetime is limited by collisions. We make three assumptions: (i) the lifetime depends on the r.m.s. relative group velocity of two colliding particles, v_{rel} , which for a chain is $\sqrt{2}$ times the single-particle r.m.s. group velocity, (ii) the inverse lifetime is given as $\Gamma_{rel} = \rho v_{rel}$, and (iii) the density, ρ , and relative group velocity are evaluated with the full relativistic dispersion of the NLsM. The density is then

$$\rho(T) = \frac{3}{2\pi} \int_{-\pi}^{\pi} dq \exp\left(-\frac{\epsilon(q)}{k_B T}\right) \quad (19)$$

and the root mean square relative group velocity of particles in one dimension is

$$v_{rel}(T) = \sqrt{2} \sqrt{\frac{3}{2\pi\rho(T)} \int_{-\pi}^{\pi} dq \left(\frac{v_s^2 q}{\epsilon(q)}\right)^2 \exp\left(-\frac{\epsilon(q)}{k_B T}\right)}. \quad (20)$$

The integrals are not analytically solvable and were calculated numerically to obtain the collision frequency $\Gamma_{rel}(T) = \rho(T)v_{rel}(T)$ independent of the cutoff π . Equation (20) corrects an error in the width formula in Ref. 22. For relativistic particles the collision frequency is increased by the larger density at large momentum, and decreased by their single-particle r.m.s. group velocity, which saturates at less than v_s . The relative group velocity directly included in Eq. (20) through the factor $\sqrt{2}$ is largely responsible for the higher collision frequency.

The two estimates of the half-width are shown in Fig. 4. The general trend confirms that the model of Damle and Sachdev (solid line) describing an antiferromagnetic spin-1 chain at $T < \Delta$ as a dilute gas of Haldane excitations is basically correct.²⁷ A somewhat closer agreement with experiment is given by the free-particle calculation we have performed (dashed line), which is closely similar to the result using the measured crystal dispersion. Our calculation may be valid to slightly higher temperatures because we have retained the full NL σ M dispersion. However, below $T < 10$ K the measured excitation widths are higher than the calculations. This is probably due to the interchain spin correlations which soften the Haldane gap near the ordering wave vector (0.33, 0.33, 1), so that there is an increased thermal population of excitations.

B. Temperature dependence of solitonic excitations in quantum-disordered phase

An antiferromagnetic spin-1 Heisenberg chain does not order at any finite temperature and the spin-spin correlations decay exponentially with distance. However, there is a form of hidden spin order given by a nonlocal string order parameter first proposed by Den Nijs and Rommelse.⁴⁰ It is defined as

$$\mathcal{O}_{string}^{\alpha}(\mathcal{H}) = \lim_{|i-j| \rightarrow \infty} \langle \sigma_{ij}^{\alpha} \rangle_{\mathcal{H}}, \quad (21)$$

where

$$\sigma_{ij}^{\alpha} = -S_i^{\alpha} \exp\left(i\pi \sum_{l=i+1}^{j-1} S_l^{\alpha}\right) S_j^{\alpha}. \quad (22)$$

Kennedy and Tasaki⁴¹ showed the hidden spin order can be regarded as consequences of the breaking of the $Z_2 \times Z_2$ symmetry. It was shown that $\mathcal{O}_{string}^{\alpha}(\mathcal{H}) = 0.374$ for an antiferromagnetic chain with nearest-neighbor Heisenberg interactions.⁴²⁻⁴⁴ The hidden spin order can be pictured in the framework of the valence solid bond (VBS),¹⁰ where the $S=1$ spins are obtained by symmetrizing two $S=1/2$ spins on one site, and each of the $S=1/2$ spins forms a coherent

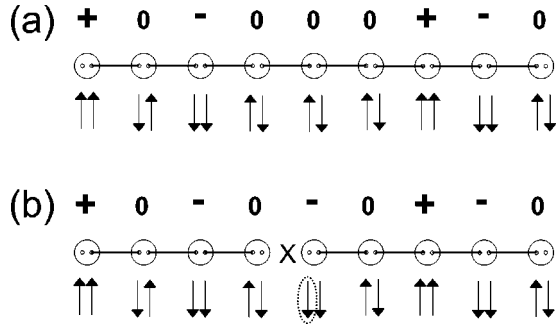


FIG. 17. (a) VBS ground state where the spin-1 (large circles) can be pictured as two symmetrized spin-1/2 (small circles within the large circles). Two spin-1/2 from neighboring sites form singlet bonds (straight lines between two spin-1/2). The picture shows one possible spin-1/2 configuration in the ground state and the corresponding spin-1 configuration showing the hidden spin string order. (b) VBS state after a neutron has transferred $S^z = -1$ to a spin-1, creating a symmetrized triplet state between two spin-1/2 on neighboring sites (the cross between two spin-1/2). This breaks the hidden spin-1 order.

singlet state with another $S = 1/2$ spin from a neighboring site. A possible VBS spin configuration for the ground state is shown in Fig. 17(a) together with its configuration in the spin-1 picture. The $S_z = 1$ and $S_z = -1$ states alternate with a random number of $S_z = 0$ states in between, and the ground state can be viewed as diluted spin-1 Néel order, which is the string order parameter defined above. In VBS $\mathcal{O}_{\text{string}}^\alpha(\mathcal{H}) = \frac{4}{9}$. This value is higher than that for the Heisenberg model because quantum fluctuations reduce the long-range hidden order in the latter.

A scattered neutron excites a spin-1/2 pair into a symmetric triplet state, as shown in Fig. 17(b). The corresponding spin configuration in the spin-1 picture shows that the dilute spin-1 Néel order is now broken. FÁTH and SÓLYOM have shown that such triplet states are moving hidden domain walls and are one-soliton excitations of the string-ordered ground state.⁹

At finite temperature, the hidden non-local string order is destroyed because spin flips are allowed through thermal population of the Haldane band that change the instantaneous magnetization of the chain. Yamamoto and Miyashita⁴⁵ introduced a local (short-range) hidden order parameter

$$\mathcal{O}_{\text{SR}} = \frac{N(+ -) + N(- +) - N(+ +) - N(- -)}{N(+ -) + N(- +) + N(+ +) + N(- -)} \quad (23)$$

where $N(\pm \mp)$ and $N(\pm \pm)$ are the total number of nearest spin pairs of $(\pm \mp)$ and $(\mp \mp)$ type, respectively. The operator is applied to a spin wave function, for example $(\dots - 0 + - 0 + 0 - 0 + - 0 + 0 - \dots)$, where all spin projection 0 are omitted, leaving $(\dots - + - + - + - \dots)$. The expectation value $\langle \mathcal{O}_{\text{SR}} \rangle$ is 1 in the absence of $(+ +)$ and $(- -)$ pairs which can be regarded as domain walls.

While the nonlocal string order collapses at any finite temperature, the local string order decreases only slowly with increasing temperature,⁴⁵ and reduces only by a factor

of 2.7 from $T = 0$ to 50 K. We note that $S(Q_c = 1)$ grows by 1.5 between 50 and 12 K and is not too much less than the factor of 2 growth of the local string order.⁴⁵ In the light of the persistence of the hidden spin order to high temperatures it is tempting to interpret the observed excitations as moving domain walls of the spin string order, and it is less surprising that they are resonant at such high temperatures. More theoretical work is needed to clarify this point, and to describe the energy and the lifetime of these high-temperature solitons.

C. High-temperature paramagnetic scattering

In the high-temperature limit $J\beta = J/k_B T \ll 1$, the second moment of the dynamic structure factor is given by³⁸

$$\langle \omega^2 \rangle = \frac{-\sum_{i,j} \exp[i\mathbf{Q}(\mathbf{R}_i - \mathbf{R}_j)] \langle [S_i^\alpha, \mathcal{H}], S_j^\alpha \rangle}{\beta \langle S_{\mathbf{Q}}^\alpha S_{-\mathbf{Q}}^\alpha \rangle}. \quad (24)$$

The thermal average of the spin-spin correlations is

$$\langle S_i^\alpha S_j^\delta \rangle = \text{Tr}[\exp(-\beta\mathcal{H}) S_i^\alpha S_j^\delta] / \text{Tr}[\exp(-\beta\mathcal{H})]. \quad (25)$$

To first order in β ,

$$\langle S_i^\alpha S_i^\delta \rangle = \delta_{\alpha,\delta} \frac{1}{3} S(S+1) \quad (26)$$

and

$$\langle S_i^\alpha S_j^\delta \rangle = -\delta_{\alpha,\delta} \beta \left(\frac{1}{3} S(S+1) \right)^2 J(\mathbf{R}_i - \mathbf{R}_j). \quad (27)$$

Please note that we use a different definition of J than that used by Lovesey.³⁸ The Fourier transform of the spatial spin-spin correlations $\langle S_i^\alpha S_j^{\alpha'} \rangle$ is

$$\langle S_{\mathbf{Q}}^\alpha S_{-\mathbf{Q}}^{\alpha'} \rangle = \frac{1}{3} S(S+1) \left(1 - \frac{1}{3} \beta S(S+1) J(\mathbf{Q}) \right). \quad (28)$$

For a 1D magnet with a nearest-neighbor exchange J , $J(\mathbf{Q}) = 2J \cos(\pi Q_c)$ and the second moment becomes

$$\langle \omega^2 \rangle = \frac{4}{3} \frac{S(S+1)}{1 - \frac{1}{3} \beta S(S+1) J(Q_c)} J^2 [1 - \cos(\pi Q_c)]. \quad (29)$$

This result can be directly compared with the measurements at $T = 200$ K. The calculated $S(Q_c)$ given by Eq. (28) with $J = 2.28$ meV is in excellent agreement with the experiment at $T = 200$ K (Fig. 16) if an overall scaling factor is fitted to the experimental data.

A more sensitive test of the theory is a quantitative comparison of the predicted and measured second energy moment. The square root of the second moment $\Omega = \langle \omega^2 \rangle^{1/2}$ was determined numerically from the measured spectra after the usual corrections were made. Figure 18 shows that $\Omega(Q_c)$ has a maximum which approaches $Q_c = 1$ at high temperatures. The solid line shows the predicted $\Omega(Q_c)$ according to

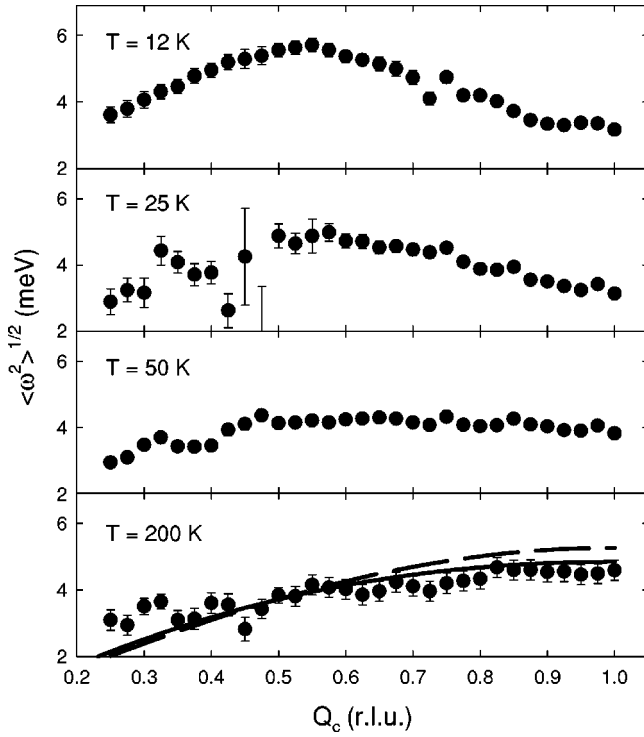


FIG. 18. Square root of the second energy moment $\Omega(Q_c)$ for several temperatures as a function of wave-vector transfer Q_c . The solid line is the theoretical prediction given by Eq. (29). The dashed line is the prediction for infinite temperature.

Eq. (29) at $T=200$ K and using $J=2.28$ meV. There is good quantitative agreement between theory and experiment considering that the solid line is not a fit but a prediction based only on the temperature and the exchange constant along the chain. $\Omega(Q_c)$ for infinite temperatures $\beta=0$ is shown by the dashed curve for comparison.

Figure 18 also shows that the maximum in $\Omega(Q_c)$ changes from $Q_c=1$ to $Q_c=0.5$ on cooling. At $T=12$ K, the maximum is where the dispersion has its largest energy. The moments of the spin spectrum are summarized in Table I. Here the integrals are done only over the positive energy response.

VI. CONCLUSIONS

In summary, the evolution of the dynamic spin structure factor $S(Q_c, \omega)$ of CsNiCl_3 has been surveyed between $T=5$ and 200 K over a wide range of wave-vector transfers Q_c along the chain.

The temperature dependence of the correlation length $\xi(T)$ was determined from the Q_c dependence of the equal-time structure factor and the results are in agreement with quantum Monte Carlo calculations except for $T < 10$ K,

close to the ordering temperature T_N . At these temperatures and at the noncritical 1D wave vector $(0.81, 0.81, 1)$ the correlation length is shorter than is predicted for isolated chains, and the gap is higher than expected. Surprisingly, the intensities of the excitations do not scale with the $1/\omega$ law which is typical for antiferromagnets. These results are in sharp contrast with the predictions of the random phase approximation and with the single mode approximation.

The magnetic excitations remain resonant and dispersive up to $T=50$ K $\approx 2J$, a temperature comparable with the spin-band width. They remain resonant because the energy of the spin excitations renormalizes upward more rapidly than their damping. The temperature dependence of the dispersion along the chain direction was measured, and the excitation energy $\Delta(T)$ and the spin velocity $v_s(T)$ were determined for $6 \text{ K} < T < 50 \text{ K}$. We found that the relation $\xi = \sqrt{v_s^2 + \alpha^2/4}/\Delta$, which is predicted by the single mode approximation, remains valid in the entire temperature region. This suggests that the excitation spectrum around the antiferromagnetic point consists of single-particle excitations even at $T=50$ K where the excitations are broad. It also hints at the existence of a hidden spin order which carries the propagating excitations as predicted by numerical calculations. The observed excitations may be regarded as domain walls (solitons) of the hidden string order, whose energy scale is J rather than Δ .

At $T=200$ K the scattering is well described as paramagnetic scattering and extends to ~ 10 meV energy transfer at the antiferromagnetic point. The upper boundary of the paramagnetic scattering exhibits a broad maximum at the antiferromagnetic point.

The structure factor and the second energy moment are consistent with the first-order high-temperature series expansion. These results call for an extension to higher temperatures of the theory for gapped weakly-coupled spin chains.

ACKNOWLEDGMENTS

We would like to thank Dr. O. Petrenko for his assistance with experiments at ISIS and Dr. P. Santini and Dr. D. A. Tennant for enlightening discussions. We are grateful to K. N. Clausen and the staff of Risø National Laboratory for their expert assistance and for the use of the excellent neutron facilities that made this research possible, regrettably no longer available with the shutdown of DRB. Financial support for the experiments was provided by the EPSRC, by the EU through its Large Installations Program, and by the British Council-National Research Council Canada Program. ORNL is managed for the U.S. DOE by UT-Battelle, LLC, under Contract No. DE-AC05-00OR22725. One of the authors (M.K.) was supported by the Swiss National Science Foundation under Contract No. 83EU-053223.

- ¹L.D. Faddeev and L.A. Takhtajan, *Phys. Lett.* **85A**, 375 (1981).
²F.D.M. Haldane, *Phys. Rev. Lett.* **50**, 1153 (1983).
³F.D.M. Haldane and M.R. Zirnbauer, *Phys. Rev. Lett.* **71**, 4055 (1993).
⁴R. Botet and R. Julien, *Phys. Rev. B* **27**, 613 (1983).
⁵M.P. Nightingale and H.W.J. Blöte, *Phys. Rev. B* **33**, 659 (1986).
⁶W.J.L. Buyers, R.M. Morra, R.L. Armstrong, M.J. Hogan, P. Gerlach, and K. Hirakawa, *Phys. Rev. Lett.* **56**, 371 (1986).
⁷M. Steiner, K. Kakurai, J.K. Kjems, D. Petitgrand, and R. Pynn, *J. Appl. Phys.* **61**, 3953 (1987).
⁸J.P. Renard, L.P. Regnault, and M. Verdaguer, *J. Phys. (France)* **49**, 1425 (1988).
⁹G. Fátth and J. Sólyom, *J. Phys.: Condens. Matter* **5**, 8983 (1993).
¹⁰I. Affleck, *J. Phys.: Condens. Matter* **1**, 3047 (1989).
¹¹D.A. Tennant, T.G. Perring, R.A. Cowley, and S.E. Nagler, *Phys. Rev. Lett.* **70**, 4003 (1993).
¹²W.J.L. Buyers, Z. Tun, A. Harrison, J.A. Rayne, and R.M. Nicklow, *Physica B* **180&181**, 222 (1992).
¹³I.A. Zaliznyak, L.-P. Regnault, and D. Petitgrand, *Phys. Rev. B* **50**, 15 824 (1994).
¹⁴A. Zheludev, S.E. Nagler, S.M. Shapiro, L.K. Chou, D.R. Talham, and M.W. Meisel, *Phys. Rev. B* **53**, 15 004 (1996).
¹⁵H. Mutka, C. Payen, P. Molinié, J.L. Soubeyroux, P. Colombet, and A.D. Taylor, *Phys. Rev. Lett.* **67**, 497 (1991).
¹⁶J. Darriet and L.-P. Regnault, *Solid State Commun.* **86**, 409 (1993).
¹⁷H. Mutka, C. Payen, P. Molinié, and R.S. Eccleston, *Physica B* **213&214**, 170 (1995).
¹⁸T. Sakaguchi, K. Kakurai, T. Yokoo, and J. Akimitsu, *J. Phys. Soc. Jpn.* **65**, 3025 (1996).
¹⁹J.P. Renard, M. Verdaguer, L.-P. Regnault, W.A.C. Erkelens, J. Rossat-Mignod, J. Ribas, W.G. Stirling, and C. Vettier, *J. Appl. Phys.* **63**, 3538 (1988).
²⁰S. Ma, D.H. Reich, C. Broholm, B.J. Sternlieb, and R.W. Erwin, *Phys. Rev. B* **51**, 3289 (1995).
²¹R.M. Morra, W.J.L. Buyers, R.L. Armstrong, and K. Hirakawa, *Phys. Rev. B* **38**, 543 (1988).
²²M. Kenzelmann, R.A. Cowley, W.J.L. Buyers, and D.F. McMorrow, *Phys. Rev. B* **63**, 134417 (2001).
²³A.A. Katori, Y. Ajiro, T. Asano, and T. Goto, *J. Phys. Soc. Jpn.* **64**, 3038 (1995).
²⁴H. Kadowaki, K. Ubukoshi, and K. Hirakawa, *J. Phys. Soc. Jpn.* **56**, 751 (1987).
²⁵N. Achiwa, *J. Phys. Soc. Jpn.* **27**, 561 (1969).
²⁶K. Lefmann, D.F. McMorrow, H.M. Ronnow, K. Nielsen, K.N. Clausen, B. Lake, and G. Aeppli, *Physica B* **283**, 343 (2000).
²⁷K. Damle and S. Sachdev, *Phys. Rev. B* **57**, 8307 (1998).
²⁸M.J. Cooper and R. Nathans, *Acta Crystallogr.* **23**, 357 (1967).
²⁹T. Jolicœur and O. Golinelli, *Phys. Rev. B* **50**, 9265 (1994).
³⁰M. Kenzelmann, R.A. Cowley, W.J.L. Buyers, Z. Tun, R. Coldea, and M. Enderle, *Phys. Rev. B* **66**, 024407 (2002).
³¹M. Kenzelmann, R.A. Cowley, W.J.L. Buyers, R. Coldea, J.S. Gardner, M. Enderle, D.F. McMorrow, and S.M. Bennington, *Phys. Rev. Lett.* **87**, 017201 (2001).
³²Y.J. Kim, M. Greven, U.J. Wiese, and R.J. Birgeneau, *Eur. Phys. J. B* **4**, 291 (1998).
³³M. Kenzelmann and P. Santini (unpublished).
³⁴Z. Tun, W.J.L. Buyers, R.L. Armstrong, K. Hirakawa, and B. Briat, *Phys. Rev. B* **42**, 4677 (1990).
³⁵M. Kenzelmann *et al.* (unpublished).
³⁶P.C. Hohenberg and W.F. Brinkman, *Phys. Rev. B* **10**, 128 (1974).
³⁷P. G. Gennes, *Magnetism*, edited by G. T. Rado and H. Suhl (Academic, New York, 1960), Vol. 3.
³⁸S. W. Lovesey, *Theory of Neutron Scattering from Condensed Matter* (Clarendon Press, Oxford, 1984).
³⁹S.W. Lovesey and E. Balcar, *J. Phys.: Condens. Matter* **6**, 1253 (1994).
⁴⁰M. den Nijs and K. Rommelse, *Phys. Rev. B* **40**, 4709 (1989).
⁴¹T. Kennedy and H. Tasaki, *Phys. Rev. B* **45**, 304 (1991).
⁴²S.M. Girvin and D.P. Arovas, *Phys. Scr.*, T **27**, 156 (1989).
⁴³Y. Hatsugai and M. Kohmoto, *Phys. Rev. B* **44**, 11 789 (1991).
⁴⁴S.R. White and D.A. Huse, *Phys. Rev. B* **48**, 3844 (1993).
⁴⁵S. Yamamoto and S. Miyashita, *Phys. Rev. B* **48**, 9528 (1993).